Physical Origin of Color Changes in Lutetium Hydride under Pressure

Run Lv(吕润)[1,2], Wenqian Tu(涂文倩)[1,2], Dingfu Shao(邵定夫)[1], Yuping Sun(孙玉平)[1,3,4], and Wenjian Lu(鲁文建)[1*]

[1]*Key Laboratory of Materials Physics, Institute of Solid State Physics, Hefei Institutes of Physical Science, Chinese Academy of Sciences, Hefei 230031, China*

[2]*Science Island Branch of Graduate School, University of Science and Technology of China, Hefei 230026, China*

[3]*High Magnetic Field Laboratory, Institute of Solid State Physics, Hefei Institutes of Physical Science, Chinese Academy of Sciences, Hefei 230031, China*

[4]*Collaborative Innovation Center of Microstructures, Nanjing University, Nanjing 210093, China*

(Received 19 July 2023; accepted manuscript online17 October 2023)

Recently, near-ambient superconductivity was claimed in nitrogen-doped lutetium hydride ($LuH_{3-\delta}N_{\varepsilon}$). Unfortunately, all follow-up research still cannot find superconductivity signs in successfully synthesized lutetium dihydride (LuH_2) and N-doped $LuH_{2\pm x}N_y$. However, a similar intriguing observation was the pressure-induced color changes (from blue to pink and subsequent red). The physical understanding of its origin and the correlation between the color, crystal structure, and chemical composition of Lu–H–N is still lacking. In this work, we systematically investigated the optical properties of LuH_2 and LuH_3, and the effects of hydrogen vacancies and nitrogen doping using the first-principles calculations by considering both interband and intraband contributions. Our results demonstrate that the evolution of reflectivity peaks near blue and red light, which is driven by changes in the band gap and Fermi velocity of free electrons, resulting in the blue-to-red color change under pressure. In contrast, LuH_3 exhibits gray and no color change up to 50 GPa. Furthermore, we investigated the effects of hydrogen vacancies and nitrogen doping on its optical properties. Hydrogen vacancies can significantly decrease the pressure of blue-to-red color change in LuH_2 but do not have a noticeable effect on the color of LuH_3. The N-doped LuH_2 with the substitution of a hydrogen atom at the tetrahedral position maintains the color change when the N-doping concentration is low. As the doping level increases, this trend becomes less obvious, while other N-doped structures do not show a blue-to-red color change. Our results can clarify the origin of the experimental observed blue-to-red color change in lutetium hydride and also provide a further understanding of the potential N-doped lutetium dihydride.

DOI: 10.1088/0256-307X/40/11/117401

The search for room-temperature superconductors has been a long-standing goal in condensed matter physics. According to the Bardeen–Cooper–Schrieffer theory, metallic hydrogen and hydrogen-rich compounds with light ionic mass can produce high-temperature superconductivity.[1,2] In recent years, materials such as H_3S (203 K at 155 GPa)[3,4] and LaH_{10} (250 K at 190 GPa)[5,6] have been predicted by density-functional-theory calculations and confirmed by high-pressure experiments. Unfortunately, high pressure is always indispensable for the stability and superconductivity of these compounds.[7] Recently, near-ambient superconductivity was reported in N-doped lutetium hydride $LuH_{3-\delta}N_{\varepsilon}$.[8] The authors reported that superconductivity emerges at 0.3 GPa, reaches its maximum at 1 GPa, and vanishes above 3 GPa. Interestingly, the crystal color changes from blue to pink at 0.3 GPa and subsequently to red at 3 GPa. However, the following research on lutetium dihydride LuH_2[9,10] and $LuH_{2\pm x}N_y$[7,11–13] showed no near-ambient superconductivity but observed similar color changes under pressure. Moreover, the superconductivity transition temperature (T_c) of LuH_3, considered N doping and an anharmonic effect in first-principles calculations, is much lower than room temperature.[14,15] Other lutetium hydrides, such as LuH_3[16] and Lu_4H_{23}[17] show superconductivity below 12 K (122 GPa) and 71 K (218 GPa), respectively.

Undoubtedly, the microscopic crystal structure and chemical composition of lutetium hydride and its N-doped compounds are still controversial. However, the color change observed in several experiments is generally consistent. Color is a basic property of materials and is determined by their optical reflectivity to light with different wavelengths. Different structures and chemical compositions have different electronic properties, which determine their optical properties, such as reflection and absorption. Therefore, the color and its changes under pressure can provide basic information about the electronic structure of the material, which can be used as important evidence to study its structure and chemical composition. Several theoretical studies[18–21] have shown that LuH_2 exhibits the blue-to-red color change consistent with experimental

*Corresponding author. Email: wjlu@issp.ac.cn

© 2023 Chinese Physical Society and IOP Publishing Ltd

reports, and the concentration of H vacancies can influence the pressure of color changes.[18] However, the physical origin of the blue-to-red color change is not fully clear. Furthermore, the possible occupation position and the effect of the doped nitrogen atom are still unknown.

In this work, we systematically investigated the optical properties of nitrogen-doped lutetium hydrides under pressure through first-principles calculations. Firstly, we investigated the optical properties of LuH_2 and LuH_3. Our results indicate that under pressure, LuH_2 undergoes a color change from blue to red, while LuH_3 maintains its gray color. Based on the dielectric function and electronic properties, we elucidate that both interband and intraband transitions are important for forming peaks of reflectivity spectra in the blue and red regions. Changes in its band gaps and Fermi velocity of free electrons drive the evolution of these peaks, resulting in the blue-to-red color change. Furthermore, we studied the influence of hydrogen vacancies and nitrogen doping on the optical properties. Hydrogen vacancies can significantly decrease the pressure of the blue-to-red color change in LuH_2. When these vacancies are abundant, the structure could exhibit a yellow color under high pressure. However, hydrogen vacancies do not have a significant impact on the color of LuH_3 under pressure. N-doped lutetium dihydride, $Lu_{18}H_{35}N$ ($LuH_{1.944}N_{0.056}$), with N replacing H at the tetrahedral site, exhibits a similar trend in reflectivity and blue-to-red color change. When the doping concentration of the N atom is higher, the color change becomes less obvious. However, the other five N-doped compounds considered in this work show no similar color change. The present results suggest that lutetium dihydride with N at the tetrahedral site is a potential structure of nitrogen-doped lutetium hydride. Additionally, we calculated the phonon dispersion under different pressures and also considered anharmonic effects. The phonon dispersions indicate that LuH_2 is dynamically stable, while LuH_3 is unstable under near-ambient conditions.

Calculation Details. The first-principles calculations based on the density functional theory were performed by the Vienna *ab initio* Simulation Package (VASP).[22,23] The pseudopotential was described by using projector augmented wave methods, and exchange-correlation interaction was treated by generalized gradient approximation, which is parameterized by Perdew–Burke–Ernzerhof version.[24] The plane-wave kinetic cut-off energy was set to 500 eV. Both lattice parameters and atom positions were fully optimized. The Brillouin zone was sampled with an $18\times18\times18$ k-points mesh for structural optimization. The electronic properties calculation used a $40\times40\times40$ k-points mesh for LuH_2 and LuH_3 and at least a $10\times10\times10$ k-points mesh for N-doped superstructures. Convergence criteria for energy and force were set to 10^{-8} eV and 10^{-3} eV/Å, respectively. The dielectric function (only for interband contribution) was calculated by the independent particle approximation using the same k-points mesh with electron properties. For metals, the dielectric function has contributions from both interband and intraband transitions. The interband contribution describes all allowed direct transitions, defined as

$$\varepsilon^{\text{inter}}(\omega) = \varepsilon_1^{\text{inter}}(\omega) + i\varepsilon_2^{\text{inter}}(\omega).$$

It was post-processed with a VASPKIT code.[25] The imaginary part of the 3×3 dielectric tensor is defined as[26]

$$\varepsilon_{2,\alpha\beta}^{\text{inter}}(\omega) = \frac{4\pi^2e^2}{\Omega}\lim_{q\to0}\frac{1}{q^2}\sum\nolimits_{c,v,\boldsymbol{k}} 2w_k\delta(\epsilon_{c\boldsymbol{k}} - \epsilon_{v\boldsymbol{k}} - \omega) \times \langle u_{c\boldsymbol{k}+\boldsymbol{e}_\alpha\boldsymbol{q}}|u_{v\boldsymbol{k}}\rangle\langle u_{c\boldsymbol{k}+\boldsymbol{e}_\beta\boldsymbol{q}}|u_{v\boldsymbol{k}}\rangle^*,$$

where the indices c and v denote the conduction and the valence band states that w_k donates the weight of the k points, and $\boldsymbol{e}_\alpha$ and $\boldsymbol{e}_\beta$ are three Cartesian directions. The real part of the interband part is related to the imaginary part by the Kramers–Kronig relation[26]

$$\varepsilon_{1,\alpha\beta}^{\text{inter}}(\omega) = 1 + \frac{2}{\pi}\,\text{P}\int_0^\infty \frac{\varepsilon_{2,\alpha\beta}^{\text{inter}}(\omega')\omega'}{\omega'^2-\omega^2}d\omega',$$

where P represents the principal value.

The intraband part was calculated by using the Drude model,[27,28]

$$\varepsilon^{\text{intra}}(\omega) = \varepsilon_1^{\text{intra}}(\omega) + i\varepsilon_2^{\text{intra}}(\omega),$$
$$\varepsilon_1^{\text{intra}}(\omega) = 1 - \frac{\omega_{\text{p}}^2}{\omega^2+\Gamma^2},$$
$$\varepsilon_2^{\text{intra}}(\omega) = \frac{\omega_{\text{p}}^2\Gamma}{\omega^3+\omega\Gamma^2},$$

where ω_{p} and Γ represent plasma frequency and relaxation rate, respectively. Here we select a typical value $\Gamma = 0.2$, and obtain ω_{p} as follows:

$$\omega_{\text{p},\alpha\beta}^2 = \frac{4\pi e^2}{V\hbar^2}\sum\nolimits_{n,k} 2g_k\frac{\partial f(E_{n,k})}{\partial E}\left(\boldsymbol{e}_\alpha\frac{\partial E_{n,k}}{\partial k}\right)\left(\boldsymbol{e}_\beta\frac{\partial E_{n,k}}{\partial k}\right),$$

where V denotes the volume of the unit cell, g_k is the weight of the k points, f is the occupancy, E is the band energy, $\boldsymbol{e}_\alpha$ and $\boldsymbol{e}_\beta$ denote three directions. Finally, we can reach the total dielectric function

$$\varepsilon(\omega) = \varepsilon^{\text{inter}}(\omega) + \varepsilon^{\text{intra}}(\omega).$$

Then, the optical reflectivity is calculated by[29]

$$R(\omega) = \left|\frac{\sqrt{\varepsilon(\omega)}-1}{\sqrt{\varepsilon(\omega)}+1}\right|^2.$$

The colorimetry theory[30] is used to calculate the color of materials. Based on the reflectivity $R(\omega)$, the power distribution of reflected light under the D_{65} standard illumination (simulates daylight) can be expressed as

$$P(\omega) = P_{\text{D}_{65}}(\omega)\times R(\omega).$$

Then, the tristimulus values (R, G, B), i.e., the color coordinates, are calculated by

$$R = \int_{380}^{780} P(\lambda)\bar{r}(\lambda)d\lambda,$$
$$G = \int_{380}^{780} P(\lambda)\bar{g}(\lambda)d\lambda,$$
$$B = \int_{380}^{780} P(\lambda)\bar{b}(\lambda)d\lambda.$$

Here, λ represents the wavelength; $\bar{r}(\omega)$, $\bar{g}(\omega)$ and $\bar{b}(\omega)$ are color-matching functions corresponding to the (R, G, B) tristimulus space.

Results and Discussions. We first calculated the dielectric function of LuH_2 and LuH_3. The dielectric function reveals fundamental electronic structure information and determines optical properties, such as reflection and absorption. The color of the material can then be derived from the reflectivity. The dielectric function of interband transitions consists of a real part and an imaginary part. The imaginary part represents all allowed direct transitions from occupied to unoccupied states. The real and imaginary parts are related by the Kramers–Kronig relation.[26] Black lines in Figs. 1(b) and 1(d) show the interband dielectric function of LuH_2 at 0 GPa. Considering that LuH_2 is a metal, intraband transitions also contribute to the dielectric function. The Drude free electron model[27,28] is used to describe the intraband part. The blue dashed lines in Figs. 1(b) and 1(d) represent the contribution of intraband transitions to the dielectric function. Compared to the dielectric function without intraband transitions, the inclusion of the intraband part significantly affects the imaginary dielectric function below 3 eV. Its effect on the real dielectric function is below 5 eV, due to the plasma frequency of 5.82 eV. The calculated total dielectric function is also in good agreement with the experimental[31] and theoretical reports.[18–21] Figure 1(c) shows the reflectivity of LuH_2 at 0 GPa. If only interband transitions are considered, the reflectivity exhibits little variation within the visible light range, as shown by the black line. However, when intraband transitions are taken into account, a peak appears in the blue light region, and only a narrow energy range with high reflectivity near red light. Therefore, blue light is predominantly reflected, and the material has a blue appearance, which is also consistent with previous theoretical reports.[18,19]

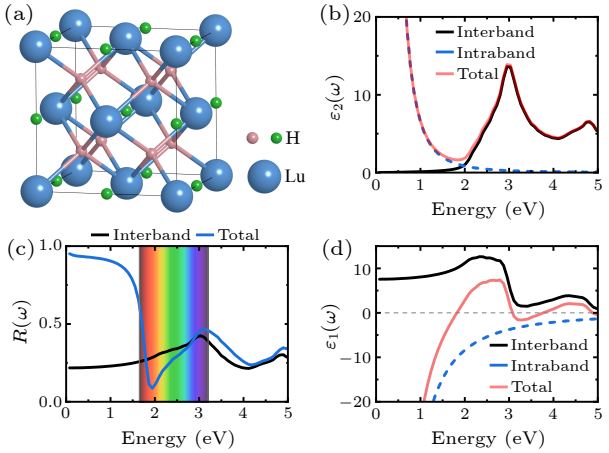


Fig. 1. (a) Crystal structure of lutetium hydride with the fluorite structure ($Fm\bar{3}m$). The pink and green H atoms occupy tetrahedral and octahedral sites, respectively. The structure of LuH_3 contains pink and green H atoms, while that of LuH_2 only contains pink H atoms. The calculated imaginary part ε_2 (b) and real part ε_1 (d) of the dielectric function of LuH_2. (c) Reflectivity $R(\omega)$ spectra of LuH_2.

To explore the pressure-induced color changes, we calculated the dielectric function and reflectivity under different pressures. Figure 2(a) shows the imaginary and real parts of the total dielectric function. The plasma frequencies under different pressures are listed in Table S1 in the Supplemental Material. For the imaginary part ε_2 of the total dielectric function, its peak moves to higher energy when pressure increases, resulting in a decrease around 3 eV. This is mainly contributed by interband transitions. Below 2 eV, there is a slight increase, contributed by both interband and intraband transitions, as shown in Fig. 3(a). The real part ε_1 also shifts its peak to higher energy and decreases below 3 eV. These changes result in a variation of the reflectivity, as shown in Fig. 2(b). Under higher pressure, the reflectivity of blue light gradually decreases, while the reflectivity of red light increases. Consequently, the color of LuH_2 shifts to violet at $\sim$20 GPa and to red at $\sim$30 GPa. The reflectivity in 1.8 eV (red light) and 2.8 eV (blue light) under different pressures are listed in Table S1. The calculated color displayed in Fig. 2(c) is well consistent with the experimental observation[7] in Fig. 2(d). We also noted a difference in the pressure of color transition between calculations and observations in Refs. [9,10,13]. This discrepancy will be discussed in the section related to hydrogen vacancies.

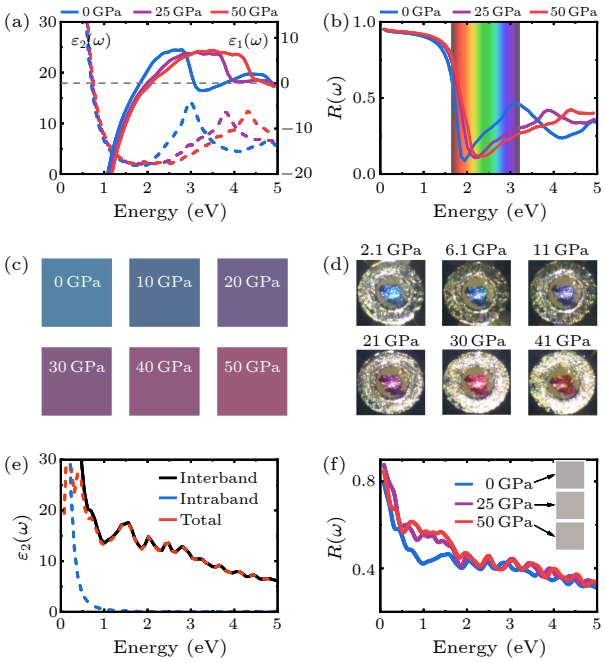


Fig. 2. (a) Imaginary part ε_2 (dashed line) and real part ε_1 (solid line) of the dielectric function of LuH_2 under different pressures. (b) Reflectivity spectra $R(\omega)$ of LuH_2. (c) Calculated color and (d) experimentally observed optical microscope images of LuH_2 under different pressures (from Ref. [7]). (e) Imaginary part of the dielectric function of LuH_3. (f) Reflectivity spectra $R(\omega)$ of LuH_3 under different pressures. Insets show the corresponding color.

To investigate whether LuH_3 could exhibit a similar color change, we calculated its dielectric function, reflec-

tivity, and color under different pressures. Figure 2(e) shows the imaginary part of the dielectric function of LuH_3 at 0 GPa. The plasma frequency of LuH_3 is 1.62 eV (the plasma frequencies at other pressures are also listed in Table S1 in the Supplemental Material). As a result, intraband transitions contribute to the dielectric function of LuH_3 mainly below 1 eV, which is lower than the energy range of visible light. Therefore, the total dielectric function in the visible light energy range is mainly determined by interband transitions. Moreover, the dielectric function within the energy range of visible light shows slight variation and does not have a prominent peak, resulting in a small variation of reflectivity in this range. Using its reflectivity, we calculated the color of LuH_3 under different pressures and found that it remains gray, as displayed in the inset of Fig. 2(d). This is consistent with a previous report.[18]

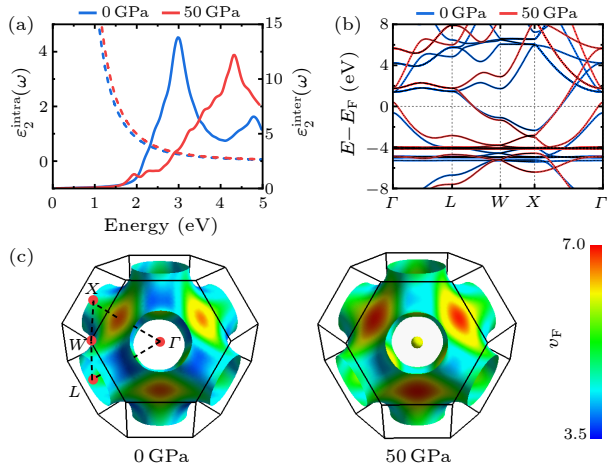


Fig. 3. (a) Imaginary part of the dielectric function contributed by interband (solid line) and intraband (dashed line) transitions, (b) band structure, and (c) Fermi surface of LuH_2 under 0 and 50 GPa.

To gain a deeper understanding of the physical origin of the change in optical properties, we analyze the electronic structure of LuH_2. In Fig. 2(a), the imaginary part of the total dielectric function increases around 1.8 eV and decreases around 2.8 eV, resulting in color changes. These changes can be attributed to interband and intraband transitions, as shown in Fig. 3(a). Compared to the blue solid line (0 GPa), the peak of the red solid line (50 GPa) moves to 4.3 eV, resulting in a decrease of reflectivity in 2.8 eV. Around 1.8 eV, the red solid line shows a slight increase. In its band structure, the bandgap at the W point increased from 2.8 eV to 4.3 eV, while the bandgap at the Γ point decreased from 2.0 eV to 1.8 eV. These changes correspond to the variations in interband transitions. The imaginary part of the intraband transitions, represented by the red dashed line, shows a slight increase at 1.8 eV. However, its contribution to the real part is significant, as shown in Fig. S1 of the Supplemental Material. This is attributed to an increase in the Fermi velocity of electrons on the Fermi surface, leading to a higher plasma frequency ($\omega_{\rm p}$) (listed in Table S1). Figure 3(c) shows the Fermi surface of LuH_2 at 0 GPa and 50 GPa, with red indicating regions for high Fermi velocity. The increase in Fermi velocity is accompanied by a decrease in effective mass, which results in higher electron mobility. This causes LuH_2 to exhibit better metallic behavior at higher pressures.[7]

In some experimental reports,[7,8,11–13] the hydrogen is non-stoichiometric, and the pressure of color changes is lower than our calculated results. Therefore, we calculate the optical properties of LuH_2 and LuH_3 with different ratios of hydrogen vacancies. Figure 4 shows the calculated results. Figures 4(a), 4(c), and 4(e) are the reflectivity of LuH_2 with different ratios of H vacancies under different pressures. Compared with LuH_2, $LuH_{1.875}$ has a higher reflectivity for red light under the same pressure, so its blue-to-red color change can occur at a lower pressure. As the ratio of H vacancies in LuH_2 continues to increase, such as $LuH_{1.750}$ and $LuH_{1.625}$, the calculated results show that its reflectivity near yellow light increases under high pressure, causing the color changing to yellow. This different color change has been observed in Ref. [10]. Similar results have also been reported in previous calculations on LuH_2 with H vacancies.[18,19] Next, we calculated LuH_3 with different ratios of H vacancies, as shown in Figs. 4(b), 4(d), and 4(f). In these results, H vacancies moderate change its reflectivity. However, there is still not a dominant peak within the visible light energy range, resulting in a gray appearance with no significant changes under pressure.

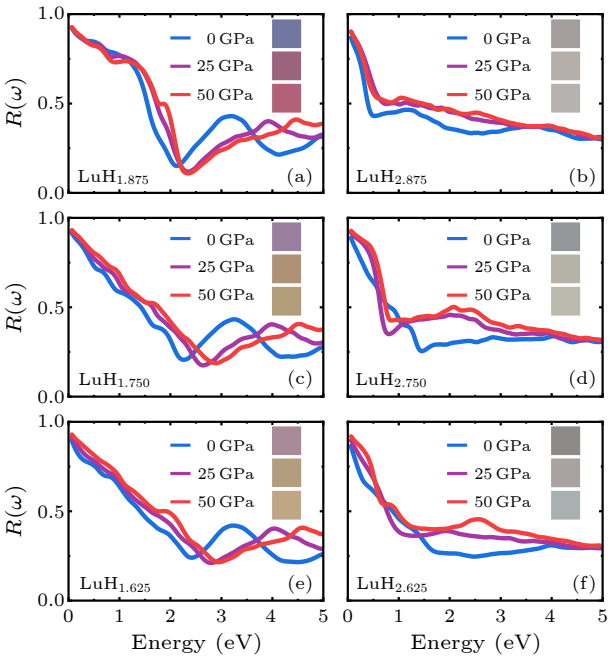


Fig. 4. Reflectivity of LuH_2 with different ratios of H vacancy: (a) $LuH_{1.875}$, (c) $LuH_{1.750}$, and (e) $LuH_{1.625}$. Reflectivity of LuH_3 with different ratios of H vacancy: (b) $LuH_{2.875}$, (d) $LuH_{2.750}$, and (f) $LuH_{2.625}$. Insets show the color at the corresponding pressure.

Furthermore, we considered the effect of different N doping on the color of Lu–H–N compounds. As shown in Fig. 1(a), there are two types of H atom positions in

the $Fm\bar{3}m$ structure of lutetium hydride: tetrahedral and octahedral sites. For LuH_2, nitrogen can replace an H atom at the tetrahedral site or occupy the octahedral site. Firstly, we simply considered doping one N atom into a $2 \times 2 \times 2$ supercell of LuH_2, which can form $Lu_8H_{15}N$ ($LuH_{1.875}N_{0.125}$) and $Lu_8H_{16}N$ ($LuH_2N_{0.125}$). We calculated their dielectric function, reflectivity, and color. The reflectivity and color of these materials under different pressures are shown in Figs. 5(a) and 5(b). Compared to LuH_2, there was no significant color change from blue to red. However, the reflectivity of $Lu_8H_{15}N$ in the visible light range exhibits a similar distribution and evolution to that of LuH_2. Our results align with those reported in Ref. [18]. Under high pressure, the reflectivity of the blue light decreases while that of the red light increases. In contrast, the reflectivity of $Lu_8H_{16}N$ does not exhibit the above characteristics. This similar trend in reflectivity of $Lu_8H_{15}N$ under high pressure inspired us to consider that, at lower N doping concentrations, it may be possible to exhibit a significant color change similar to LuH_2. Therefore, we considered replacing one H atom with an N atom in a $3 \times 3 \times 2$ supercell of LuH_2, forming $Lu_{18}H_{35}N$ ($LuH_{1.944}N_{0.056}$). Figure 5(c) shows that $Lu_{18}H_{35}N$ could exhibit a very similar trend of reflectivity and color change under different pressures. These results suggest that the doped N atoms are more likely to be located at the tetrahedral positions.

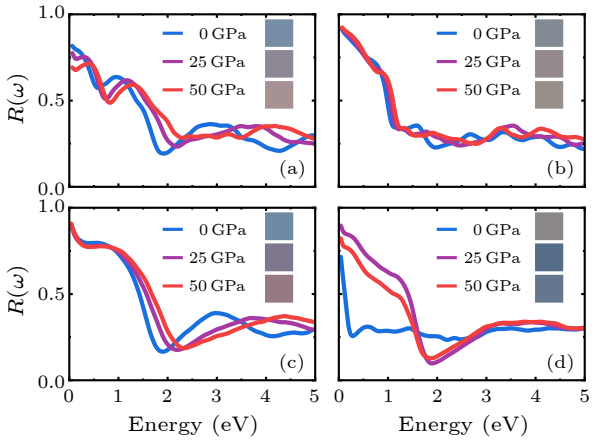


Fig. 5. Reflectivity of (a) $Lu_8H_{15}N$ ($LuH_{1.875}N_{0.125}$, nitrogen atom at the tetrahedral site), (b) $Lu_8H_{16}N$ ($LuH_2N_{0.125}$, nitrogen atom at the octahedral site), (c) $Lu_{18}H_{35}N$ ($LuH_{1.944}N_{0.056}$, nitrogen atom at the tetrahedral site), (d) $Lu_8H_{23}N$ ($LuH_{2.875}N_{0.125}$, nitrogen atom at the tetrahedral site). Insets show the color at the corresponding pressure.

Next, we adopted four structures for N-doped LuH_3 that were previously suggested in Ref. [32]. These compounds have a high density of states near the Fermi energy, which can benefit the occurrence of superconductivity.[32] However, the calculated colors of these four compounds do not exhibit the blue-to-red color change. Figure 5(d) shows the reflectivity of $Lu_8H_{23}N$ ($LuH_{2.875}N_{0.125}$), where one H atom is replaced by an N atom at the tetrahedral site in a $2 \times 2 \times 2$ supercell of LuH_3. Under pressure, it shows a similar distribution to that of LuH_2, but it does not have a similar evolution. Figures S5(b) and S5(c) in the Supplemental Material show its dielectric function at 25 GPa. Intraband transitions mainly contribute below 1.5 eV, similar to LuH_3. Thus, $Lu_8H_{23}N$ with N at the tetrahedral site retains its blue color under high pressures. The other three compounds exhibit gray color under different pressures (see Figs. S6–S8 in the Supplemental Material). All considered structures and related dielectric functions of the N-doped lutetium hydrides are displayed in the Supplemental Material.

Additionally, we calculated the phonon dispersion of LuH_2 and LuH_3 to investigate their structural stability. Figures S15(a) and S15(b) show that LuH_2 is dynamically stable from 0 GPa to 50 GPa, while LuH_3 is unstable at low pressures (< 25 GPa). For LuH_3, as pressure is higher than 25 GPa, the imaginary frequency vanishes. Using the mode decomposition technique developed in the DynaPhoPy code,[33] we also calculated the anharmonic phonon dispersion at 300 K. The comparison with harmonic and anharmonic phonon dispersion is shown in Figs. S15(c) and S15(d). When anharmonic effects are included, the phonon dispersion of LuH_2 shows only minor corrections. For LuH_3, most of the imaginary frequencies have vanished, but large imaginary frequencies remain near the W point, indicating its instability. The above results are consistent with the previous report on the thermodynamic stability of lutetium hydride.[34]

In summary, we have investigated the optical properties of LuH_2 and LuH_3, as well as the effects of hydrogen vacancies and nitrogen doping lutetium hydrides under different pressures. By calculating the dielectric function and reflectivity, we find that LuH_2 can reproduce the pressure-induced color changes observed in experiments. Both interband and intraband transitions contribute to the formation of reflectivity peaks in the blue-light and red-light regions. Under high pressure, the increase in the direct energy gap at the W point, the decrease in the gap at the Γ point, and the increase in the Fermi velocity of free electrons cause the reflectivity of blue light to decrease and that of the red light to increase, resulting in the blue-to-red color change. Furthermore, we study the influence of hydrogen vacancies and nitrogen doping. Hydrogen vacancies can significantly decrease the pressure of blue-to-red color change in LuH_2, and abundant vacancies lead to a yellow appearance under pressure. However, hydrogen vacancies do not have an obvious impact on the color of LuH_3 under different pressures. The results of different N-doped compounds show only lutetium dihydride, with N replacing H at the tetrahedral site, which could exhibit a similar trend of color changes of LuH_2 when the doping concentration of the N atom is low. Other N-doped compounds show no similar color change. Additionally, our calculated phonon dispersions show that LuH_3 is dynamically unstable under near-ambient conditions. Our results clarify the physical origin of the pressure-induced blue-to-red color change of lutetium hydride observed in experiments and provide further understanding of the potential N-doped

lutetium dihydride.

Acknowledgment. This work was supported by the National Key Research and Development Program of China (Grant Nos. 2022YFA1403203 and 2021YFA1600200), and the National Natural Science Foundation of China (Grant Nos. U2032215 and 12241405).

References

[1] Ashcroft N W 1968 *Phys. Rev. Lett.* **21** 1748
[2] Ashcroft N W 2004 *Phys. Rev. Lett.* **92** 187002
[3] Duan D *et al.* 2014 *Sci. Rep.* **4** 6968
[4] Drozdov A P *et al.* 2015 *Nature* **525** 73
[5] Drozdov A P *et al.* 2019 *Nature* **569** 528
[6] Wang C, Yi S, and Cho J H 2020 *Phys. Rev. B* **101** 104506
[7] Ming X *et al.* 2023 *Nature* **620** 72
[8] Dasenbrock-Gammon N *et al.* 2023 *Nature* **615** 244
[9] Shan P F *et al.* 2023 *Chin. Phys. Lett.* **40** 046101
[10] Zhao X *et al.* 2023 *Sci. Bull.* **68** 883
[11] Zhang Y J *et al.* 2023 *Sci. China Phys. Mech. Astron.* **66** 287411
[12] Cai S *et al.* 2023 *Matter Radiat. Extremes* **8** 048001
[13] Xing X *et al.* 2023 arxiv:2303.17587 [cond-mat.supr-con]
[14] Lucrezi R *et al.* 2023 arxiv:2304.06685 [cond-mat.supr-con]
[15] Huo Z *et al.* 2023 *Matter Radiat. Extremes* **8** 038402
[16] Shao M *et al.* 2021 *Inorg. Chem.* **60** 15330
[17] Li Z *et al.* 2023 *Sci. China Phys. Mech. Astron.* **66** 267411
[18] Kim S W *et al.* 2023 arXiv:2304.07326v1 [cond-mat.supr-con]
[19] Tao X *et al.* 2023 *Sci. Bull.* **68** 1372
[20] Liu Z *et al.* 2023 arXiv:2305.06103v1 [cond-mat.supr-con]
[21] Dangić Đ *et al.* 2023 arXiv:2305.06751v1 [cond-mat.supr-con]
[22] Kresse G and Hafner J 1993 *Phys. Rev. B* **47** 558
[23] Kresse G and Furthmüller J 1996 *Phys. Rev. B* **54** 11169
[24] Perdew J P, Burke K and Ernzerhof M 1996 *Phys. Rev. Lett.* **77** 3865
[25] Wang V *et al.* 2021 *Comput. Phys. Commun.* **267** 108033
[26] Gajdoš M *et al.* 2006 *Phys. Rev. B* **73** 045112
[27] Millis A J (Baeriswyl D, Degiorgi L ed) 2004 *Strong Interactions in Low Dimensions* (Dordrecht: Springer Netherlands) p 195
[28] Zhang L *et al.* 2016 *Nat. Mater.* **15** 204
[29] Saha S, Sinha T P, and Mookerjee A 2000 *Phys. Rev. B* **62** 8828
[30] Wyszecki G and Stiles W S 1982 *Color Science: Concepts Methods, Quantitative Data and Formulae* (New York: Wiley)
[31] Weaver J H, Rosei R and Peterson D T 1979 *Phys. Rev. B* **19** 4855
[32] Denchfield A, Park H and Hemley R J 2023 arXiv:2305.18196 [cond-mat.supr-con]
[33] Carreras A, Togo A and Tanaka I 2017 *Comput. Phys. Commun.* **221** 221
[34] Xie F *et al.* 2023 *Chin. Phys. Lett.* **40** 057401